

Microstructure Evolution and Mechanical Behavior of a Hot-Rolled High-Manganese Dual-Phase Transformation-Induced Plasticity/Twinning-Induced Plasticity Steel



LIMING FU, MOKUN SHAN, DAODA ZHANG, HUANRONG WANG, WEI WANG, and AIDANG SHAN

The microstructures and deformation behavior were studied in a high-temperature annealed high-manganese dual-phase (28 vol pct δ -ferrite and 72 vol pct γ -austenite) transformation-induced plasticity/twinning-induced plasticity (TRIP/TWIP) steel. The results showed that the steel exhibits a special Lüders-like yielding phenomenon at room temperature (RT) and 348 K (75 °C), while it shows continuous yielding at 423 K, 573 K and 673 K (150 °C, 300 °C and 400 °C) deformation. A significant TRIP effect takes place during Lüders-like deformation at RT and 348 K (75 °C) temperatures. Semiquantitative analysis of the TRIP effect on the Lüders-like yield phenomenon proves that a softening effect of the strain energy consumption of strain-induced transformation is mainly responsible for this Lüders-like phenomenon. The TWIP mechanism dominates the 423 K (150 °C) deformation process, while the dislocation glide controls the plasticity at 573 K (300 °C) deformation. The delta-ferrite, as a hard phase in annealed dual-phase steel, greatly affects the mechanical stability of austenite due to the heterogeneous strain distribution between the two phases during deformation. A delta-ferrite-aided TRIP effect, *i.e.*, martensite transformation induced by localized strain concentration of the hard delta-ferrite, is proposed to explain this kind of Lüders-like phenomenon. Moreover, the tensile curve at RT exhibits an upward curved behavior in the middle deformation stage, which is principally attributed to the deformation twinning of austenite retained after Lüders-like deformation. The combination of the TRIP effect during Lüders-like deformation and the subsequent TWIP effect greatly enhances the ductility in this annealed high-manganese dual-phase TRIP/TWIP steel.

DOI: 10.1007/s11661-017-3994-0

© The Minerals, Metals & Materials Society and ASM International 2017

I. INTRODUCTION

THE high-manganese Fe-Mn-C alloys with low stacking fault energy (SFE) may exhibit either the transformation-induced plasticity (TRIP) or twinning-induced plasticity (TWIP), or both, phenomenon through adjusting alloying elements such as Mn, Al, and Si.^[1–3] These alloys are currently being developed as potential candidates for automobile applications. The TRIP/TWIP steel combines the advantages of higher strength due to the TRIP effect and better ductility due to the TWIP effect and, consequently, exhibits unique comprehensive mechanical properties. Because of these

characteristics, it has been the subject of great scientific and technological interest.^[1,4–9]

The appearance of the obvious yield point and formation of the Lüders bands during the early stage of deformation is a well-known phenomenon in many low-carbon steels.^[10–12] This deformation behavior has been explained by the Cottrell–Bilby theory, which is related to the interaction between dislocations and the atmosphere of interstitial atoms, such as C, N, and B, in steels.^[10] Moreover, a Lüders-like “yield” phenomenon (LLYP), which shows tensile curve shapes similar to those of the conventional Lüders-like phenomenon but has an essentially different deformation mechanism, has been observed in the intermetallic alloy,^[13] the NiTi shape memory alloy,^[14–16] the magnesium alloy,^[17] and the intercritically annealed cold rolling TRIP steels.^[11,18–20] Their mechanisms are attributed to the dynamic pileup of dislocations at the grain boundaries, martensite growth, deformation twinning, and stability of the retained austenite, respectively. It was found that the strain-stress curves of a number of austenitic stainless steels also display the characteristics of the LLYP when deformed at cryogenic temperatures.^[21–23] It has been proven that this kind of Lüders-like behavior

LIMING FU, MOKUN SHAN, and AIDANG SHAN are with the School of Materials Science and Engineering, Shanghai Jiao Tong University, 800 Dongchuan Road, Shanghai 200240, P.R. China. Contact e-mails: lmfu@sjtu.edu.cn and adshan@sjtu.edu.cn DAODA ZHANG is with the Jiangxi Mechanical Science Institute, 125 Dinggong Road, Nanchang, 330002, Jiangxi Province, P.R. China. HUANRONG WANG and WEI WANG are with the Baosteel Research Institute, 889 Fujin Road, Shanghai 201900, P.R. China.

Manuscript submitted October 4, 2016.

Article published online February 21, 2017

is directly associated with the metastable austenite to strain-induced martensite (SIM) transformation.^[21,22] In contrast, rather limited works are focused on the study of the yielding behavior in high-manganese steels. High-manganese TRIP/TWIP steel is actually a metastable material at RT, because the strain-induced transformation often takes place in the initial stage of the plastic deformation when macrostrains are applied.^[7]

In this article, we studied a special type of LLYP with great plastic instability and large yielding strain in the early stage of plastic deformation during the macroscopic tensile tests in a high-manganese dual-phase (delta-ferrite + austenite) TRIP/TWIP steel. It was found that the formation of this phenomenon is closely associated with strain-induced transformation. Moreover, a systematic work was undertaken for in-depth understanding of the microstructure evolution and the mechanical behavior during deformation in this dual-phase TRIP/TWIP steel, and an attempt at a theoretical analysis was made to evaluate the TRIP effect on the Lüders-like deformation behavior. Considering that the temperature greatly influences the SFE values, and thus leads to the change in the active plasticity mechanism of steel,^[1,2,4,20,24–30] the present article also evaluated the deformation modes at various deformation temperatures in this dual-phase high-manganese TRIP/TWIP steel.

II. EXPERIMENTAL

The steel with a chemical composition of Fe-20Mn-3.8Al-2.6Si-0.082C (wt pct) was smelt in a 50-kg vacuum induction furnace. After being homogenized at 1523 K (1250 °C) for 2 hours under a protective argon atmosphere, the ingot was hot rolled to a plate of 15-mm thickness [finish temperature was 1173 K (900 °C)] and then water quenched. Tensile specimens with the dimensions shown in Figure 1 were machined from the plate. A tensile test with a constant strain rate of $5 \times 10^{-4} \text{ s}^{-1}$ at various temperatures was performed on a Gleeble 3800 [Dynamic Systems Inc. (DSI), America] thermo-mechanical simulator, followed by annealing treatment with 25 K/s heating rate to 1323 K (1050 °C), holding for 15 minutes, and cooling with 10 K/s to the RT.

X-ray diffraction (XRD) measurements at a scan rate of 0.5 deg/s with a Cu target were made to identify the coexisting phases in the samples. The XRD specimens sectioned from the identical position of tensile samples were chemically polished in a solution consisting of H₂O (15 mL) + H₂O₂ (15 mL) + HF (1 mL) + C₂H₂O₄ (1 g) before measurements to eliminate the effects of cutting and polishing.

In order to study the stability of the delta-ferrite in this study, laser scanning confocal microscopy (type VL2000DX-SVF17SP, Lasertec Corporation, Japan) was used to *in-situ* observe the change of delta-ferrite during the process of high-temperature annealing. Microstructural observation was carried out by optical microscopy (OM), scanning electron microscopy (SEM), and transmission electron microscopy (TEM). Energy-dispersive X-ray spectroscopy (EDS), along with

SEM, was employed to examine compositional analysis. The specimens for observation were all taken from the center of the section in the tensile samples. The volume delta-ferrite was measured by an image analysis system at magnification 250 times, and 20 pictures were selected for each specimen. Thin foils for TEM were obtained by a twin-jet polisher in a 7 pct HClO₄ and 93 pct ethanol solution at 248 K (–25 °C).

III. RESULTS AND DISCUSSION

A. Microstructures and Mechanical Properties

1. Deformation behavior for different temperatures

Figure 2 displays the strain-stress curves of annealed specimens tensioned at various temperatures. It is seen that the tensile curves at room temperature (RT) and 348 K (75 °C) exhibit an obvious LLYP, especially for specimens at RT, where a remarkable stress drop and a large strain plateau appear in the early deformation stage. Our previous study showed that this special LLYP is essentially associated with SIM transformation.^[9] However, the tensile curves at 423 K and 573 K (150 °C and 300 °C) deformation show continuous yielding; *i.e.*, no obvious yield drop occurs. The ultimate tensile strength (UTS) and uniform elongation (UE) decrease with increasing deformation temperature, except for the specimen at 423 K (150 °C) deformation, where ductility is obviously enhanced.

Figure 3 shows the typical optical microstructures of the dual-phase TRIP/TWIP steel before and after deformation at different temperatures, respectively. The initial microstructure of the experimental steel before tensile comprises ferrite, austenite, and some annealing twins (Figure 3(a)). These microstructural characteristics are quite similar to the other duplex TWIP steels reported in the literature.^[31,32] It is clear that the austenite matrix is severely deformed after tensile. Many deformation twins and some very fine plates (maybe martensite) are observed in the austenite matrix after RT deformation (Figure 3(b)). By contrast, these plates or deformation twins in the austenite at 423 K (150 °C) deformation become relatively smaller than those of RT deformation (Figure 3(c)) and are rarely observed in the austenite matrix at 573 K (300 °C) deformation.

In order to reveal the deformation behaviors at various temperatures, the XRD measurements were carried out on the annealed specimens subjected to a strain of 9.5 pct, which approaches the maximum value of the strain-hardening rate after the Lüders-like region in RT deformation. The XRD patterns of the annealed specimens at various temperatures and the change of austenite volume fraction in this strain level are shown in Figure 4. It can be seen clearly from Figure 4(a) that, in comparison to the unstrained annealed specimen, the ϵ phase peak appears and the intensity ratio of the (110) α and (111) γ peaks is markedly enhanced at RT and 348 K (75 °C) deformation, which clearly indicates that the SIM transformation occurs in this strain level at these two temperatures of deformation. However,

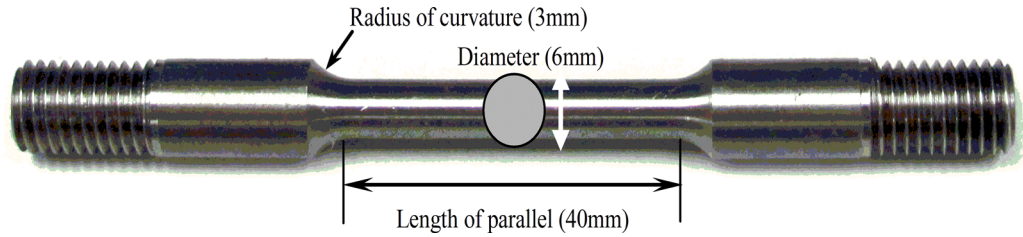


Fig. 1—Shape and dimension of the tensile testing specimens.

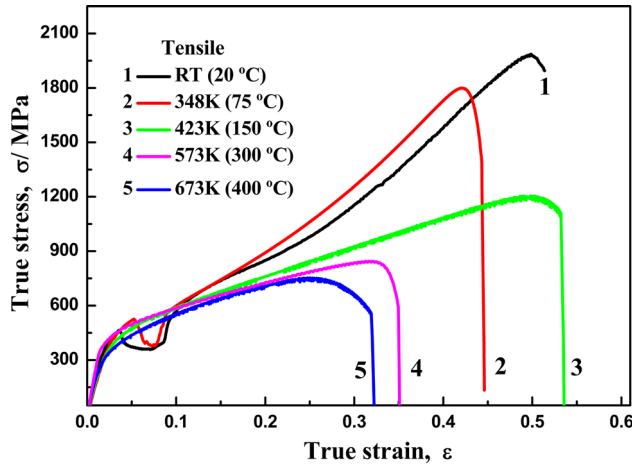


Fig. 2—True stress–strain curves of specimens tensioned at various temperatures.

except for the existence of the preferential orientation in the γ phase at 573 K (300 °C), no obvious changes in α and ϵ peaks are observed at 423 K and 573 K (150 °C and 300 °C) deformation. It is evident from Figure 4(b), which displays the change in the austenite volume fraction for the annealed specimens strained to 9.5 pct at various temperatures of deformation, that the austenite fraction is substantially reduced at RT and 348 K (75 °C) deformation but is virtually unchanged at 423 K and 573 K (150 °C and 300 °C). These results indicate that this annealed dual-phase steel exhibits different deformation behaviors at various temperatures.

2. Microstructural evolution during the RT deformation

The annealed steel deformation exhibits high UTS and substantially enhanced ductility at RT. In order to obtain detailed knowledge and reveal these deformation

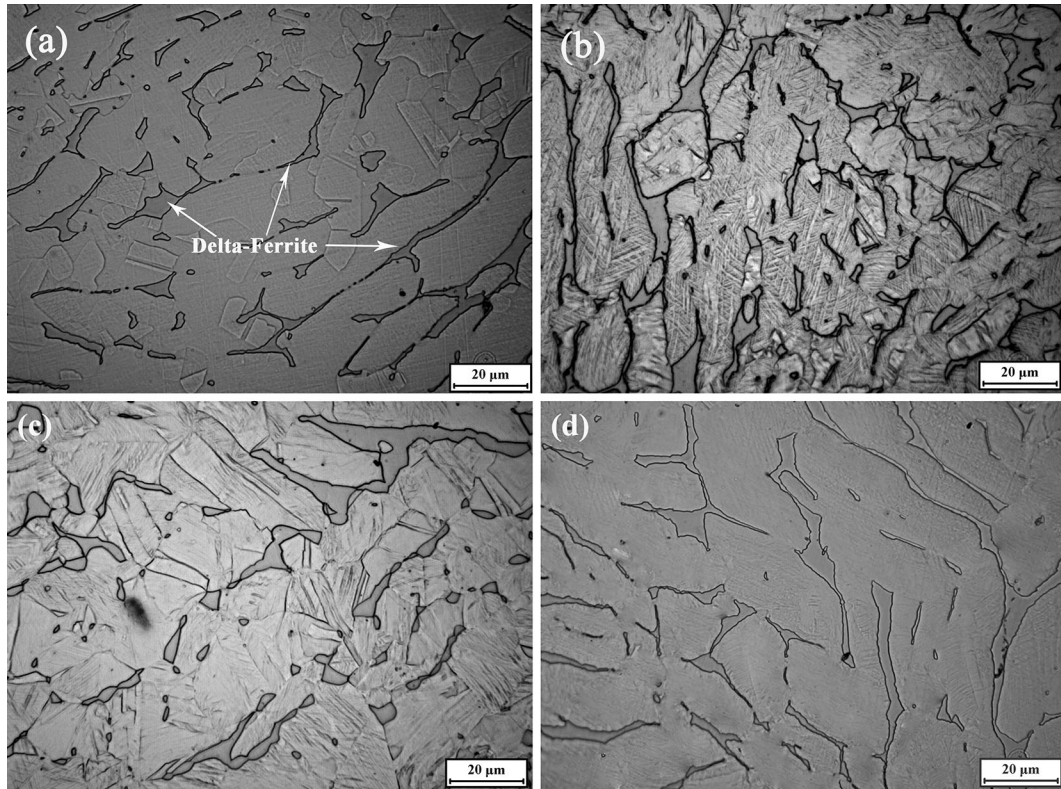


Fig. 3—Typical OM image of the dual-phase TRIP/TWIP steel: (a) prior to deformation, (b) after deformation at RT, (c) at 423 K (150 °C), and (d) at 573 K (300 °C).

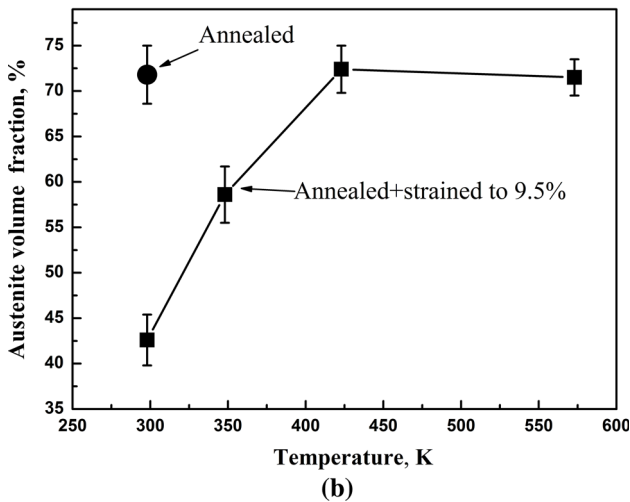
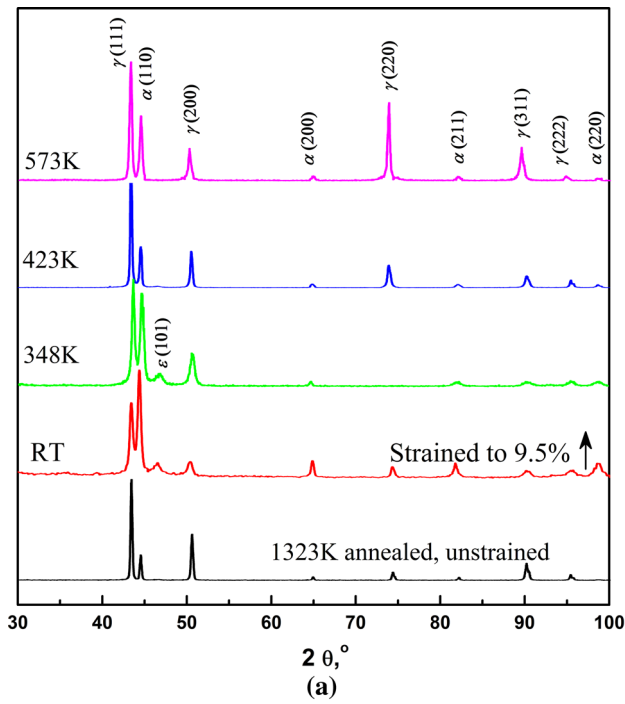


Fig. 4—Graphic showing (a) the XRD patterns of the annealed specimens strained to 9.5 pct at various temperatures and (b) the change of austenite volume fraction in this strain level.

behaviors, the present work studied the microstructure evolution during the RT deformation process based on the analysis of XRD measurements.

The tensile curves clearly demonstrate a special LLYP in the early deformation stage and an upward-curvature phenomenon with a gradual increase in strain-hardening rate ($d_2\sigma/d\varepsilon^2 > 0$) in the later deformation stage, as shown in Figure 5(a), where the strain-hardening rate ($d\sigma/d\varepsilon$) is obtained from the derivation of the tensile curve after a 10-point smoothing treatment. In this figure, three important strain values are highlighted: yield strain ε_Y ; a critical strain ε_C , after which the plastic deformation becomes unstable; and ε_R , a strain of the inflection point in the tensile curve at which the hardening rate, $d\sigma/d\varepsilon$, arrives at the maximum value.

According to the characteristics of the strain-hardening rate, the true stress–strain curve is readily divided into six stages, as indicated by the vertical dot line in Figure 5(a). The first stage (stage 1) is the elastic deformation; the second stage (stage 2) is the beginning of the plastic deformation. In this stage, the strain-hardening rate decreases rapidly to zero, but the stress increases with the strain increase from ε_Y to ε_C . The tensile curve from ε_C to ε_R is defined as stage 3. Once the strain reaches ε_C , the plastic deformation becomes unstable and the stress quickly declines to a stress plateau. At the end of the stress plateau, the stress begins to sharply increase as the strain increases, and the corresponding strain-hardening rate is also strongly accelerated until the inflection point strain ε_R arrives. Evidently, deformation stage 3 actually experiences a process from elastoplastic instability to plastic re-stability. Hereafter, we term the tensile curve of deformation stage 3 as the Lüders-like “yield” region (LLYR). However, it is seen from the tensile curve that this type of LLYR is not strictly a yield phenomenon, as the plastic deformation, from strain of ε_Y to ε_C , evidently occurred first. After ε_R , the stress begins to slowly increase with the strain while the work-hardening rate gradually declines to a stable state (stage 4), keeps slowly increasing nearly in the middle of the deformation process (stage 5), and finally drops until rupture occurs (stage 6).

Based on the XRD measurements, Figure 5(b) presents the volume fraction of the γ -austenite, ε -martensite, and α' -martensite of the steel as a function of true strains for 1323 K (1050 °C)–annealed specimens. It is seen that the volume fraction of austenite almost remains constant with the true strain in deformation stages 1 and 2 and then is substantially reduced in the Lüders-like deformation region (stage 3). The volume fraction of ε -martensite quickly increases before strain at 7.3 pct and then declines quickly, whereas the volume fraction of α' -martensite first decreases slowly and then rises swiftly with true strain increment. Since no martensite is found before deformation (the unstrained annealed specimen, as shown in Figure 4(a)), the martensite formed in LLYR evidently should be the product of SIM transformation, *i.e.*, γ - ε/α' or γ - ε - α' transformation. These results reveal that this special LLYP, during the earlier deformation stage of the high-temperature annealed dual-phase TRIP/TWIP steel, is closely associated with the TRIP effect. After the strain, ε_R , the deformation steps into stage 4. XRD measurements show that the patterns remain almost unchanged in this stage, revealing that no further SIM transformation takes place after LLYR. Moreover, the volume fractions of phases are almost invariant in deformation stage 4 (after the stress inflection point of ε_R), although the work hardening continues, as shown in Figure 5(a), which implies that the mechanism of the deformation behavior after the stress inflection point ε_R is different from that of the TRIP effect during deformation stage 3.

Figures 6 and 7 show the SEM and TEM observations of the microstructure evolution with various strain levels in LLYR during the RT deformation, respectively. In these figures, the deformation strains of 3.6, 7.3, 9.5, and

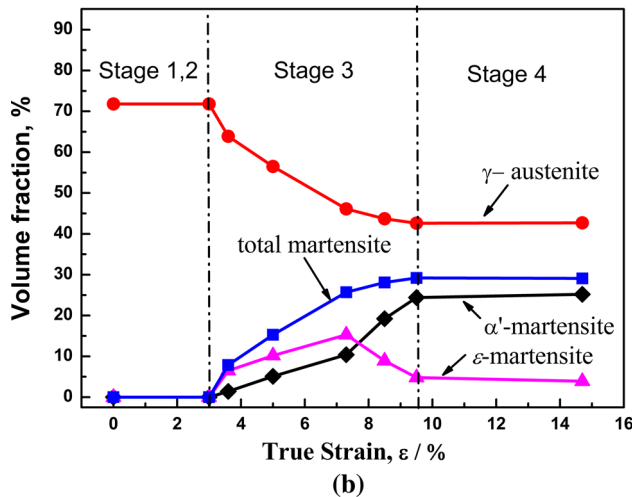
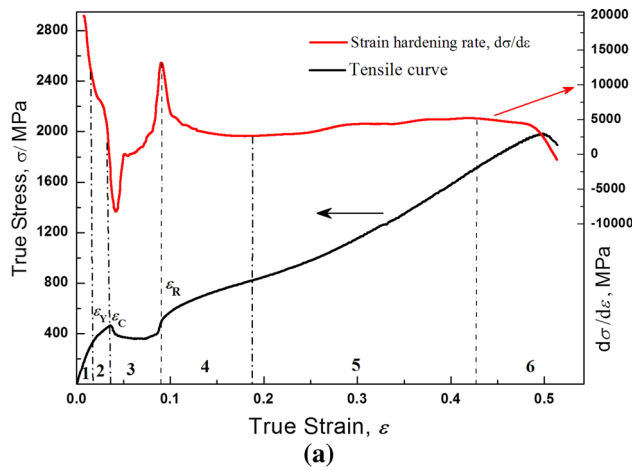


Fig. 5—Graphic showing (a) the strain-stress curve and the corresponding strain-hardening rate for an annealed specimen and (b) the changes of the volume fraction of the phases with strains.

14.7 pct, respectively, represent the beginning of the elastoplastic instability (just over ϵ_C), the middle of the stress plateau, an approach to the stress inflection point ϵ_R , and an approximation of the work-hardening stable in stage 4. It is found that the delta-ferrite phase in dual TRIP/TWIP steel remains nearly unchanged during deformation (Figure 6), while the austenite matrix is greatly affected by straining (Figures 6 and 7). Before the plastic instability point ϵ_C in stage 2, the main deformation microstructure consists of tangled dislocations and overlapped stacking faults (SFs), and no phase transformation is found in this strain level. It is evident from Figure 7(a), which shows an example of TEM microstructure with 3.6 pct strain level, that the SFs are formed in the vicinity of the delta-ferrite phase. When the sample was strained to 3.6 pct, some thin lenticular or platelike ϵ -martensite was observed in the vicinity of the delta-ferrite phase (Figure 6(a)). With a further increase in strain to 7.3 and 9.5 pct, the austenite obviously deformed and some deformation bands or plates were clearly seen in the austenite matrix, as displayed in Figures 6(b) and (c). According to the XRD analysis, most of these plates are martensites, which are

also confirmed by the micrographs of selected area electron diffraction (SAED) of TEM shown in Figures 7(b) and (c). However, it is clear that many fine deformation twins formed in the austenite matrix of the specimen subjected to 14.7 pct deformation, as indicated in Figure 6(d). The TEM micrographs in Figure 7(d) also show that some mechanical twins exist in this strain level. Therefore, the TRIP effect is no longer the dominant deformation mechanism after stage 3, and the further increase in work hardening in flow stress is mainly associated with the TWIP effect.

3. Delta-ferrite stability during the present heat treatment

As shown in Figure 3, the ferrite exhibits two typical morphologies: a relatively larger irregular plateletlike one along the grain boundary and a small regular block one in the inner austenite matrix, which homogeneously distributes in the steel. Image analysis shows that the ferrite volume fractions of the hot-rolled and 1050 °C-annealed specimens are 28.6 and 28.2 pct, respectively. Figure 8 demonstrates the microstructure *in-situ* observed during high-temperature annealing. It is shown that the morphologies of these ferrites maintain nearly unchanged and no other ferrite was found to form in austenite during high-temperature annealing, implying these ferrites are stable phase in dual-phase TRIP/TWIP steel under the present heat treating process. Therefore, these ferrites are not transformed from austenite at low temperatures after hot rolling or during the cooling of heat treatment but should be delta-ferrite formed at high temperatures before hot rolling.

Figure 9 shows the results of the chemical element distribution of the EDS scan along a typical delta-ferrite phase. Evidently, the delta-ferrite phase substantially consists of Fe, Mn, Al, and Si. In contrast with the austenite matrix, delta-ferrite is rich in Al and Si, but contains less Mn atoms, which are all evenly distributed within the phase. The TEM observation and diffraction analysis reveal the presence of the ordered DO_3 phase in the delta-ferrite phase, as shown in Figure 10. It was found that the ordered nanoscale $Fe_3(Al,Si)$ phase, which is a hard superlattice structural intermetallic phase associated with the superdislocations and anti-phase domain boundaries, can be formed and uniformly distributed inside the delta-ferrite matrix.^[33,34] Undoubtedly, these $(Fe,Mn)_3(Al,Si)$ intermetallic phases uniformly distributed within the delta-ferrite greatly stabilize the delta-ferrite. Moreover, the microhardness measurement in the present study shows the delta-ferrite phase is more than 2 times that of austenite in the annealed steel, which should also be attributed to the contribution of the formation of the DO_3 structured $(Fe,Mn)_3(Al,Si)$ phase.

B. Mechanism of the Lüders-Like Deformation

1. Semiquantitative evaluation of the softening effect of TRIP on the Lüders-like yield phenomenon

The present Lüders-like deformation is quite different from the conventional yielding phenomenon (upper or lower yield stress) occurring immediately after the elastic

deformation, since a significant plastic deformation (stage 2) has taken place in the austenite phase before plastic instability. Therefore, the well-known Cottrell–Bilby atmosphere theory^[6] may not account for this phenomenon anymore. According to the preceding experimental analysis, it is believed that the TRIP effect is mainly responsible for Lüders-like deformation. Usually, the TRIP effect involves, on the one hand, a softening effect of the transformation behavior due to the strain energy consumption of martensite formation and, on the other hand, a hardening effect of the transformed phase microstructure.^[35] The former will lead to stress downward change with strain, whereas the latter will result in an upward change in the tensile curve. From the stress point of view, the true stress increment results from the TRIP effect at the Lüders-like strain level of ε ; $\Delta\sigma(\varepsilon)$ can be expressed as

$$\Delta\sigma(\varepsilon) = \Delta\sigma_{\text{hard}}^{\text{fM}}(\varepsilon) - \Delta\sigma_{\text{soft}}^{\text{EM}}(\varepsilon) \quad [1]$$

where $\Delta\sigma_{\text{soft}}^{\text{EM}}(\varepsilon)$ is the stress decrement caused by the softening of the strain energy consumed by SIM transformation and $\Delta\sigma_{\text{hard}}^{\text{fM}}(\varepsilon)$ represents the stress increment due to the hardening of the newly formed martensite. Obviously, it is a cooperative and competitive process.

The LLYR of the present study consists of three parts: plastic instability, stress plateau, and plastic re-stability. The martensitic transformation accompanying the quick plastic instability happens only after critical strain ε_C . This implies that the strain ε_C is the minimum value for SIM transformation in the present testing condition. Once the critical strain ε_C is reached, the strain energy accumulated from ε_Y to ε_C will be suddenly released to compensate for the energy required for martensitic transformation. The original plastic deformation tendency is difficult to maintain, and the stress drop is an inevitable consequence. Moreover, the stress after instability does not immediately recover but keeps continuously dropping with the increase in strain. This implies that the hardening effect of martensite formation is less than that of the softening resulting from the consumption of the martensitic transformation energy. Evidently, the softening effect of SIM transformation dominates the stress drop process. The subsequent stress plateau occurrence followed by plastic instability indicates that a dynamic balance is reached between the decrement due to softening of transformation behavior and the increment owing to hardening of newly formed martensites. With the volume fraction of martensite further increasing, especially for the α' -martensite quick formation, the hardening of the TRIP effect gradually dominates this deformation process. As a consequence, the stress sharply increases with the strain increase and the strain-hardening rate is strongly accelerated.

The softening mechanism of the TRIP effect is an inherent characteristic of material. On the basis of the strain–stress datum, at the early stage of deformation, a rough modeling estimation, from the transformation energy point of view, was done to attempt to explain the TRIP effect on this type of Lüders-like phenomenon in this work.

If no SIM transformation occurs during the tensile process, the tensile curve can be achieved by extrapolating the tensile curve of the initial plastic deformation stage 2. The stress mixture law is widely adopted to quantify the heterogeneous material behavior. Note that each constituent in dual phases exhibits very different deformation behavior. So, in the present study, a power law with the phenomenological nonlinear function of volume fraction proposed by Gladman *et al.*^[36] was taken to estimate the extrapolating tensile curve:

$$\sigma(\varepsilon) = (1 - f_F^n)\sigma_A(\varepsilon) + f_F^n\sigma_F(\varepsilon) \quad [2]$$

where σ , σ_A , and σ_F are, respectively, the flow stresses of the constituents without the TRIP effect; ε is the true strain; f_F is the volume fraction of the ferrite; and n is a constant.

The delta-ferrite mechanical behavior is here assumed to follow a Mises yield locus and obeys the empirical Hollomon formula. On the basis of the recent physical-based models proposed by Bouaziz *et al.*,^[37,38] the flow stress of the austenite without TWIP and TRIP effects can be expressed in the form of the well-known Voce law. Therefore, the stress–strain relations of the constituents are given, respectively, by

$$\begin{aligned} \sigma_F(\varepsilon) &= k_F\varepsilon^{n_F} \\ \sigma_A(\varepsilon) &= k_A[1 - \exp(-n_A\varepsilon)] \end{aligned} \quad [3]$$

The terms k_A and n_A are material related parameters. It was found that k_A and n_A are independent of chemical composition and have constant values of 725 MPa and 4, respectively, in Fe–Mn–C alloys.^[38] The k_F and n_F are the proportional coefficient and work-hardening exponent of delta-ferrite, respectively, and they can be obtained by regression analysis of the tensile curve in the plastic deformation.

Thus, the extrapolating curve of the tensile curve without the TRIP effect was obtained, as shown by the dashed line in Figure 11. In view of the difference between the extrapolating curve and the actual tensile curve with and without the TRIP effect, the shadow area illustrated in Figure 11 may represent the transformation energy required for SIM transformation in LLYR. Then the total energy consumed by SIM transformation W_{SIM} at a definite Lüders-like strain ε_{Lx} can be numerically calculated by integrating

$$W_{\text{SIM}} = \Delta V_{\varepsilon_C \rightarrow \varepsilon_{Lx}} \int_{\varepsilon_C}^{\varepsilon_{Lx}} \{\sigma_{\text{extra}}(\varepsilon) - \sigma_{\text{exp}}(\varepsilon)\} d\varepsilon \quad [4]$$

where $\Delta V_{\varepsilon_C \rightarrow \varepsilon_{Lx}}$ is the volume change of the sample from strain ε_C to ε_{Lx} ; σ_{extra} and σ_{exp} represent the true stress for the extrapolating and experimental tensile curve at true strain, respectively.

From the thermodynamics point of view, the martensitic transformation energy can be achieved by thermodynamic calculations. Hsu^[39] reported that the free energy change of martensitic transformation under external stress can be simplified as

$$\Delta G^{A \rightarrow M} = \Delta G_{\text{chem}}^{A \rightarrow M} + 2.1\sigma_y + 900 - 0.2\sigma \quad [5]$$

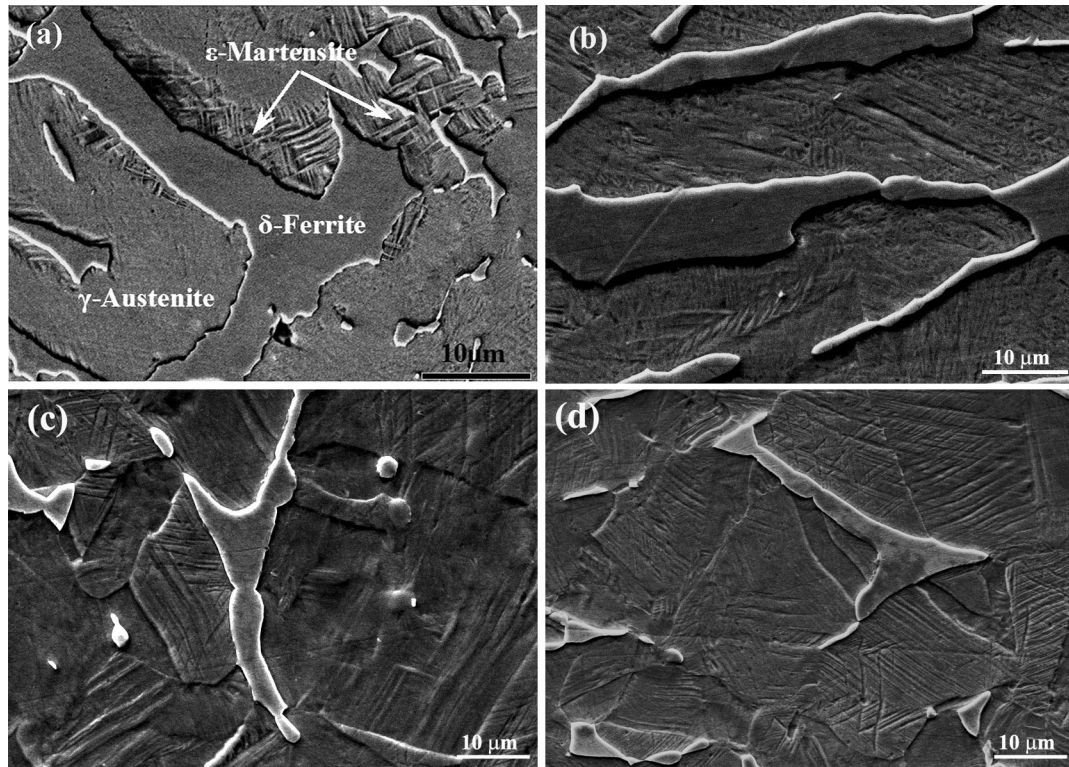


Fig. 6—SEM morphs of the 1323 K (1050 °C) annealed specimens strained to (a) 3.6 pct, (b) 7.3 pct, (c) 9.5 pct, and (d) 14.7 pct at RT.

where σ_y is the yield strength of the austenite at M_s and $\Delta G_{\text{chem}}^{\text{A} \rightarrow \text{M}}$ is the chemical free energy change of austenite to martensite transformation. In this work, the γ - ε or γ - α' transformation, or both, takes place in LLYR. For simplicity, the γ - α' transformation instead of the γ - ε - α' transformation is considered in the calculations. Therefore, $\Delta G_{\text{chem}}^{\text{A} \rightarrow \text{M}}$ can be expressed approximately as

$$\Delta G_{\text{chem}}^{\text{A} \rightarrow \text{M}} = \Delta G^{\text{A} \rightarrow \text{M}_\varepsilon} + \Delta G^{\text{A} \rightarrow \text{M}_\alpha} \quad [6]$$

where $\Delta G^{\text{A} \rightarrow \text{M}_\varepsilon}$ and $\Delta G^{\text{A} \rightarrow \text{M}_\alpha}$ are the molar free energy change accompanying austenite to ε -martensite and austenite to α -martensite transformation, respectively.

$$\Delta G^{\text{A} \rightarrow \text{M}_\varepsilon} = \sum_i x_i \Delta G_i^{\text{A} \rightarrow \text{M}_\varepsilon} + \sum_{ij} x_i x_j \Omega_{ij}^{\text{A} \rightarrow \text{M}_\varepsilon} + \Delta G_{\text{mg}}^{\text{A} \rightarrow \text{M}_\varepsilon} \quad [7]$$

in which $\Delta G_i^{\text{A} \rightarrow \text{M}_\varepsilon}$ is the molar Gibbs free energy difference between the austenite to ε -martensite phases due to the molar fractions x_i for the pure alloying element i , and $\Omega_{ij}^{\text{A} \rightarrow \text{M}_\varepsilon}$ is the interaction parameter difference for pure components i and j in the austenite and ε -martensite. The last term, $\Delta G_{\text{mg}}^{\text{A} \rightarrow \text{M}_\varepsilon}$, represents the molar Gibbs energy due the magnetic contribution of each phase. In this work, all parameters in Eq. [7] are obtained from References 29 and 30.

The chemical free energy difference of austenite to α' -martensite can be well described by^[40]

$$\Delta G^{\text{A} \rightarrow \text{M}_\alpha} = \Delta G^{\sigma=0, M_s} + \Delta S^{\sigma=0} (T - M_s) \quad [8]$$

in which $\Delta G^{\sigma=0, M_s}$ is the chemical free energy change at M_s and $\Delta S^{\sigma=0}$ is the entropy difference between the austenite and martensite. All parameters involved can be found in References 40 and 41.

Thus, the consumed energy for formation of volume fraction martensite G_{SIM} at a definite strain level can be thermodynamically estimated by

$$G_{\text{SIM}} = f_M V_M \Delta G^{\text{A} \rightarrow \text{M}} \quad [9]$$

in which f_M is the martensite volume fraction and V_M is the mole volume of martensite.

Figure 12 shows the comparison of the transformation energy between the measurements from the tensile curve and the theoretical thermodynamic calculations. It is seen that the measurements are in good agreement with the thermodynamic calculations at the range of strain from ε_C to ε_R in LLYR, which also verifies that the TRIP effect is the main reason for the result to be the Lüders-like phenomenon in the dual TRIP/TWIP steel. A slight overestimation of the measurements is probably due to the fact that the measured transformation in the shadow area also includes the extra energy for dislocation glide and the deformation of the newly formed martensite. However, a large difference was found between the measurement and the calculation after the strain ε_R . These findings also prove that the TRIP effect is not the dominant deformation mechanism after Lüders-like deformation, whereas further hardening of

the material should mainly be ascribed to the TWIP effect. It should be mentioned that the preceding results are only semiquantitative evaluations of the softening effects of SIM transformation, because the calculation only considered the static state of transformation.

2. Effect of delta-ferrite on the mechanical stability of austenite

The analysis in Section I suggests that the softening effect of martensite transformation may result in the type of LLYP observed in the present study. However, it should be noted that the value of the stress drop for plastic instability exceeds more than 100 MPa in the present study. Such a large stress drop was rarely observed in the tensile curve of low SF steels in previous works. So far, the maximum stress drop in the tensile curve of austenite stainless steel reported in the literature^[21–23] is about 50 to 60 MPa when deformed at 123 K to 77 K (−150 °C to −196 °C). Therefore, it is meaningful to find factors that lead to such significant softening of SIM transformation. Figure 6(a) shows that the ε -martensite formation is readily initiated from the region adjacent to the delta-ferrite phases when the plastic instability of Lüders-like deformation starts. This indicates that the ferrite phase plays a vitally important role in the formation of this type of LLYR in dual TRIP/TWIP steel.

Recently, Ryu *et al.*^[42] and their co-workers^[20] observed that, in medium manganese TRIP steels with a dual-phase microstructure of ferrite and austenite, a heterogeneous distribution of the plastic strain between two phases greatly affects the martensite transformation when the macroscopic strain is applied, and they concluded that the strain partitioning between phases with different mechanical properties greatly influences the mechanical stability of austenite. This result indicates that high nonuniform distribution of the internal microstrains plays an important role in the plastic deformation of the multiphase-TRIP materials, and the strain partitioning among constituent phases should be fully taken into account.

Generally, the combination of ferrite and austenite in the dual steels often leads to residual and internal stresses that influence the mechanical properties.^[43,44] A study by Shiekhelsouk *et al.*^[31] revealed that the internal stresses are in compression for ferrite but in tension for austenite at the initial state of the dual-phase TWIP steels. The austenite phase is subjected to a stress of about 600 MPa, whereas the stress in the ferritic phase is about 300 MPa for an applied macroscopic strain of about 1 pct. Their results imply that the stress in the austenite, especially in the tensile direction, is much higher than that in the ferrite during the early stage of deformation, and the stress seems more readily concentrated in austenite. These results strongly suggest that the ferrite, as a hard phase in the austenite-ferrite dual steels, is facilitated by the local strain energy accumulation when the macroscopic strain is applied, greatly affecting the mechanical stability of the austenite.

It is well known that the martensite transformation is essentially time independent, and the fraction of martensite transformation only depends on the degree of

cooling below the critical martensite start temperature.^[45] The experimental results reported in the literature^[23] show that the stress drop in Lüders-like deformation of the 304L stainless steel is about 54, 39, 35, 12, and 0 MPa (no stress drop) at 110 K, 133 K, 153 K, 223 K and 293 K (−163 °C, −140 °C, −120 °C, −50 °C and 20 °C), respectively. Evidently, the lower the austenite stability, the greater the amount of martensite that transforms and the more the stress in the process of plastic instability drops. Olson and Cohen^[46] modeled the kinetics of the strain-induced transformation. They assumed microscopic shear band intersections to be the dominant nucleation sites. The total volume fraction of martensite, f_M , depends on the number of embryos and is related to plastic strain, ε , by

$$f_M = 1 - \exp\{-\beta[1 - \exp(-\alpha\varepsilon)]^n\} \quad [10]$$

where n is a fixed exponent; α is a strain-independent constant, which depends on SFE and strain rate; and β is a parameter linearly related to the probability that an intersection generates a martensitic embryo. In this study, due to the effect of delta-ferrite strain concentration, the uniformly distributed “hard phase,” delta-ferrite, may significantly help to increase the number of embryos per unit untransformed austenite volume in the dual TRIP/TWIP steel in comparison to the single austenitic steel under strain applied. Thus, the β parameter is rapidly increased and acts as a dominant effect on the amount of martensite during Lüders-like deformation. Therefore, in terms of kinetics, the strain concentration of delta-ferrite significantly promotes the strain-induced transformation, which directly leads to the consequent plastic instability.

3. Delta-ferrite-aided SIM transformation inducing Lüders-like deformation

In this study, the ferrite plates along the austenite grain boundary and some fine ferrite islands uniformly distribute in the austenite matrix. During plastic deformation, the softer austenite phase yields first and undergoes work hardening, and then the strains are transferred onto the harder ferrite phase. The strain partitioning is, therefore, nonuniform between austenite and delta-ferrite. Due to the heterogeneous partitioning of plastic strain between two phases, the hard ferrite phase localizes the strain concentration; the austenite in the vicinity of ferrite experiencing much larger deformation than the macroelongation becomes mechanically unstable and then transforms to martensite, consequently leading to a large plastic instability. Based on the preceding results and analysis, the “delta-ferrite-assisted TRIP effect” is here proposed to describe this Lüders-like phenomenon; *i.e.*, the localized strain concentration of the austenitic matrix assisted by delta-ferrite induces SIM transformation and, thus, leads to plastic instability.

Apparently, the rapidly dispersed stress concentration and the subsequent explosive martensite transformation are two important prerequisites for the formation of this kind of Lüders-like phenomenon. The SIM transformation in the austenite matrix always preferentially takes

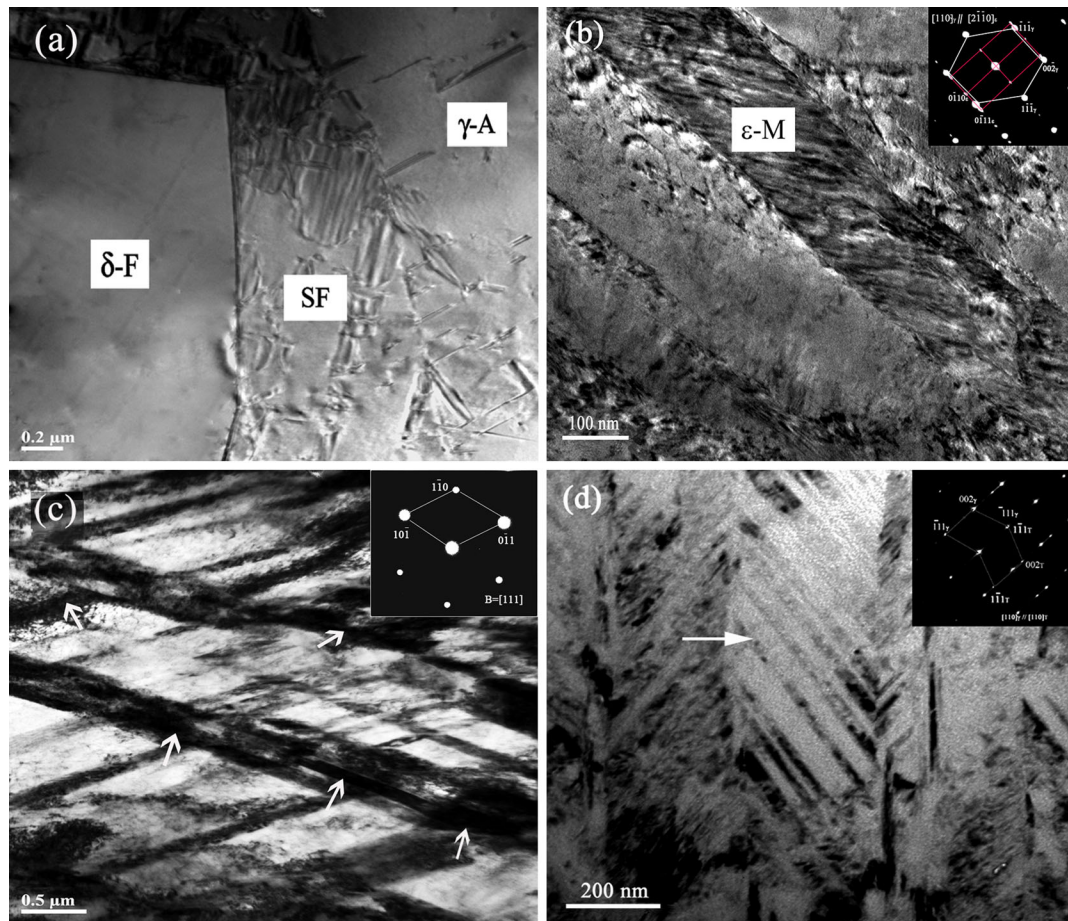


Fig. 7—Typical TEM micrographs of the specimens tensioned at RT with strain levels of (a) 3 pct; (b) 7.3 pct, SAED pattern showing the ϵ -martensite and its orientation relation with austenite; (c) 9.5 pct, the SAED pattern showing the α' -martensite plates indicated by the white arrows; and (d) 14.7 pct, the insets correspondingly showing SAED patterns of the deformation twins indicated by the white arrow.

place in the high stress concentration regions.^[47] The experiment showed that plastic deformation (stage 2) is conducted before plastic instability, indicating that the local strain concentration is highly introduced around the ferrite phase. When the local strain energy arrives at the critical energy for the martensite formation, a large amount of martensite will simultaneously form at these uniform distributed strain concentrators accompanying an instantaneous release of a large amount of strain energy consumed by transformation, resulting in a sudden drop of large true stress. Once the concentrated strain energy was released, the dynamic balance between the hardening of newly formed martensite phase and the softening of strain energy consumption due to the subsequent martensite transformation leads to a stress plateau in which the stress remains constant with the increasing strain in the tensile curve.

The SFs in austenite also play an important role in martensitic transformation. The overlapping SFs are often formed in the stress concentration region, such as the tangled dislocation, grain boundaries, and annealing twin boundaries. It is seen from Figure 8(a) that some SFs also appear adjacent to delta-ferrite, which is further evidence that the ferrite, as a hard phase in the

dual steel, promotes the concentrating stresses for the subsequent martensite transformation. It is well accepted that the γ - ϵ martensitic transformation is performed by the introduction of SFs,^[48–50] while the nucleation of α' -martensite is frequently formed at the intersections of two variants of ϵ -martensite platelets.^[2,7] The results from Figure 6 show that the γ - ϵ - α' transformation dominates the Lüders-like deformation process, which is nearly identical to the experimental results in the literature,^[7] where the γ - ϵ transformation preliminarily happens and then α' -martensite forms through the ϵ -martensite in the initial stage of plastic deformation from true strain 0.06 to 0.14.

At the end of the stress plateau, the stress begins to quickly increase with strain and the corresponding strain-hardening rate is also sharply accelerated, as exhibited in Figure 5(a). Figure 6 demonstrates that the α' -martensitic transformation begins to accelerate after the strain level approaches the end of the stress plateau in deformation stage 3. A large amount of newly formed hard α' -martensite may dramatically enhance the hardness of the austenite matrix. Therefore, it is believed that α' -martensitic transformation is mainly responsible for the acceleration of strain hardening for the plastic

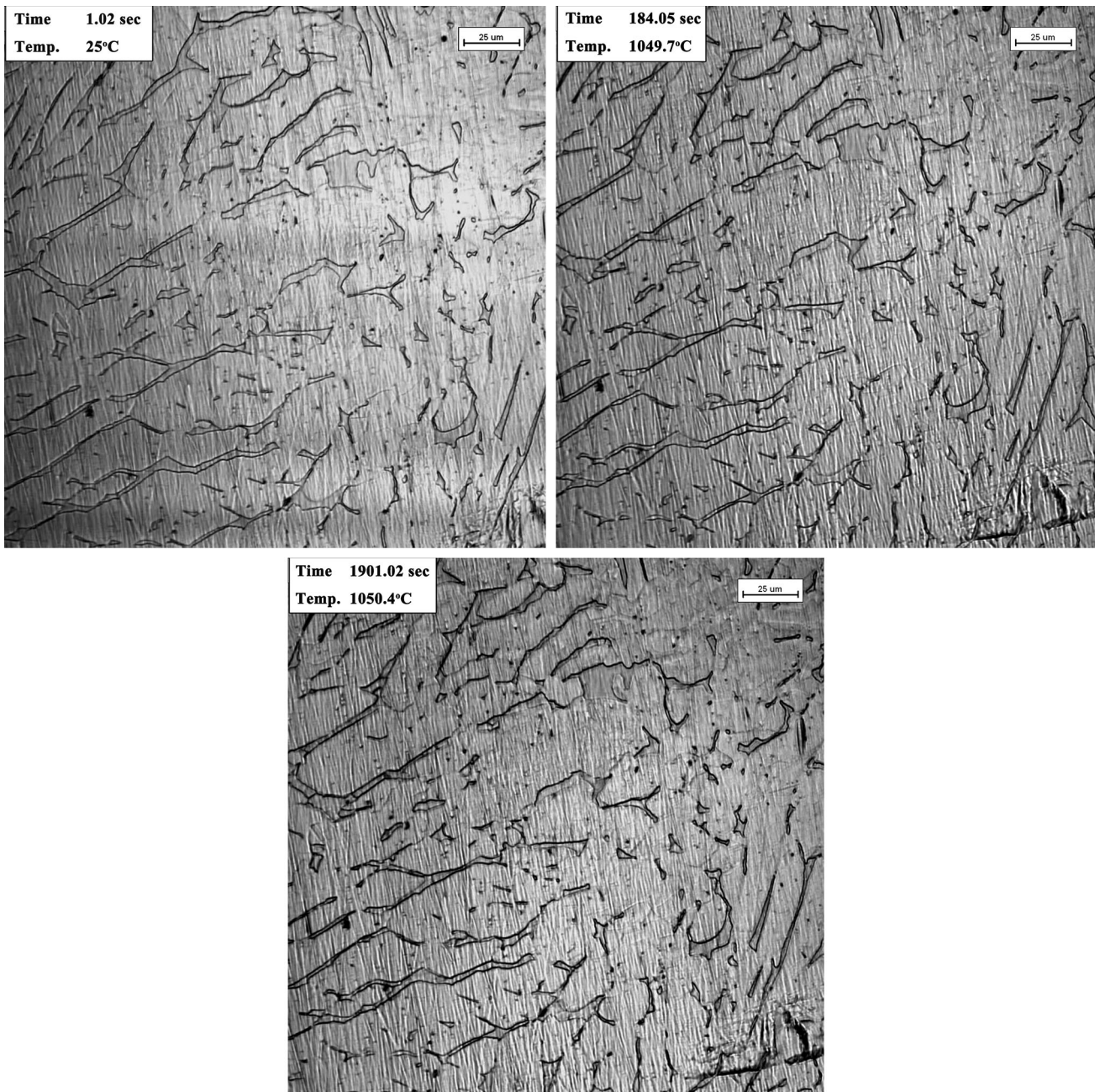


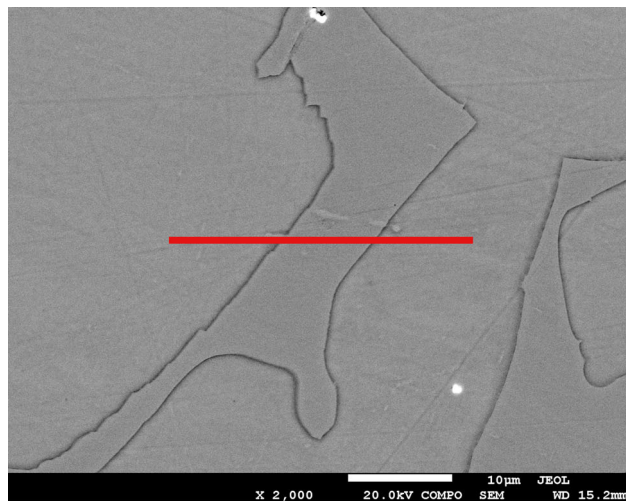
Fig. 8—*In-situ* observation of the microstructure during high-temperature annealing, showing that the delta-ferrite is a stable phase in the dual-phase TRIP/TWIP steel under the present heat treating process.

re-stability after the stress plateau in the Lüders-like region.

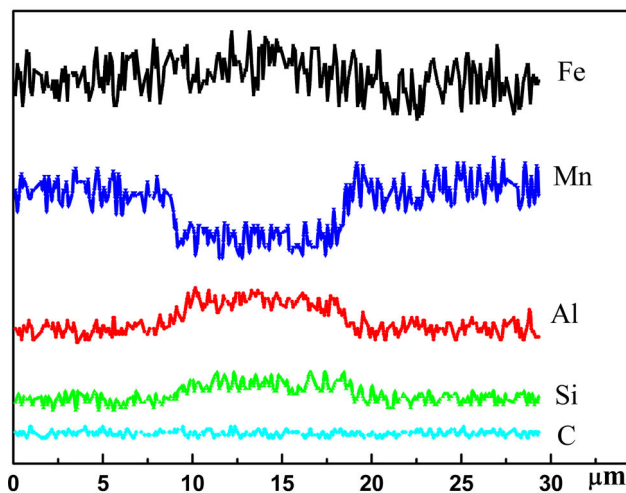
4. Upward curvature after Lüders-like deformation due to twinning

It is of interest to note that the tensile curve from Figure 3 exhibits upward curvature ($d^2\sigma/d\epsilon^2 > 0$) after the Lüders-like deformation, especially for deformation stage 5, and the work hardening is slightly enhanced, which is apparently different from the deformation behavior of the Lüders-like region. The experiments in this work indicate that twinning takes place in

deformation stages 4 and 5, as shown in Figures 6(d) and 7(d). The up-curved phenomenon is frequently observed in some high-manganese steels or alloys with lower SFE, where twinning is the key deformation mechanism.^[7,51,52] Adler *et al.*^[51] attributed this upward phenomenon to the dynamic deformation twinning. Karaman *et al.*^[52] demonstrated that the upward stress-strain response stems from the interaction between glide dislocations and the high density of twin boundaries. In Ding *et al.*'s most recent work,^[7] the similar up-curved phenomenon is also observed in the tensile curve of the 18.8 wt pct Mn TRIP/TWIP steel,



(a)



(b)

Fig. 9—Chemical element distribution of EDS scans along a typical delta-ferrite phase: (a) a typical delta-ferrite phase in 1323 K (1050 °C) annealed specimen in which the red line shows the location of line scanning and (b) chemical element distribution of EDS scans along with the line shown in (a).

where they found that twinning dominates the deformation behavior in the middle deformation stage and is the main reason for this upward phenomenon. It is believed that the TWIP effect can be considered as a dynamic Hall–Petch effect due to the fact that twinning provides a continuous refinement of the microstructure during straining, efficiently decreases the dislocation mean free path, and, thus, increases the work-hardening rate.^[53] Evidently, the upward curvature to the stress–strain curve over extensive ranges of plastic strain in TRIP/TWIP steel is also correlated with the combined effect of the softening effect of twinning and a hardening effect of the twinned microstructure.

High-manganese dual-phase TRIP/TWIP steel at RT exhibits good mechanical properties with high UTS and better elongation, which should be attributed to the coexistence of the TRIP and TWIP effects in the

steel.^[1,7,9] In our previous article, it was found that, in contrast with the hot-rolled steel, the substantial ductility enhancement without obvious strength decrement was observed for annealed steel.^[9] This indicates that, besides the TRIP effect in the Lüders-like deformation region, the twinning of the mechanically retained austenite greatly contributed to this ductility enhancement. The volume fraction of austenite remains unchanged after quick hardening deformation (Figure 5(b)), implying that the untransformed austenite becomes mechanically stable after Lüders-like deformation. The mechanical stabilization of austenite usually requires comparably large strains.^[54] Therefore, it is important for austenite to remain stable to a large strain to improve the ductility in dual-phase high-manganese steel. This interesting phenomenon provides an implication that the excellent comprehensive mechanical properties for high-manganese dual-phase steels can be achieved by adjusting the austenite behavior during deformation, some austenite transforming into martensite to enhance work-hardening capacity and preserving part of austenite to large plastic strains, which are to be deformed in twinning for further ductility enhancement.

C. Deformation Mode at Various Temperatures

It is well accepted that the SFE, which mainly depends on temperature and chemical composition, can strongly affect the deformation mode in high-manganese steel.^[1,2,20,24–30] It is reported that, with decreasing SFE, the active plasticity mode will include dislocation glide, mechanical twinning, and then martensitic transformation.^[26] Since the SFE increases with temperature, the sequence of the deformation mode is considered to occur with an increasing testing temperature. The present tensile curves at various temperatures exhibit different deformation behaviors, and the XRD analysis from Figure 4 shows different stabilities of austenite at various temperature deformation values. According to the XRD analysis and microstructural observation, the characteristics of the deformation behavior of the annealed dual-phase TRIP/TWIP steel at each deformation temperature are summarized in Table I.

1. SFE evaluation in the austenite phase at various temperatures

Based on Hirth’s proposal,^[55] the SFE can be expressed by

$$\text{SFE} = 2\rho\Delta G^{\gamma-\varepsilon} + 2\sigma^{\gamma/\varepsilon} \quad [11]$$

where ρ is the molar surface density along $\{111\}$ planes, $\Delta G^{\gamma-\varepsilon}$ is the free energy change, and $\sigma^{\gamma/\varepsilon}$ is the interfacial energy of the γ/ε interface. The free energy change and the molar surface density were extracted from other articles.^[24,29,30] The interfacial energy $\sigma^{\gamma/\varepsilon}$ is usually taken as a constant value in most works.^[26,29,30,56] However, the interfacial energy is closely related to the temperatures and chemical composition and, thus, to the SFE. Based on the experimental results in the Fe–Mn system reported by Volosevich *et al.*^[57] the interfacial energy,

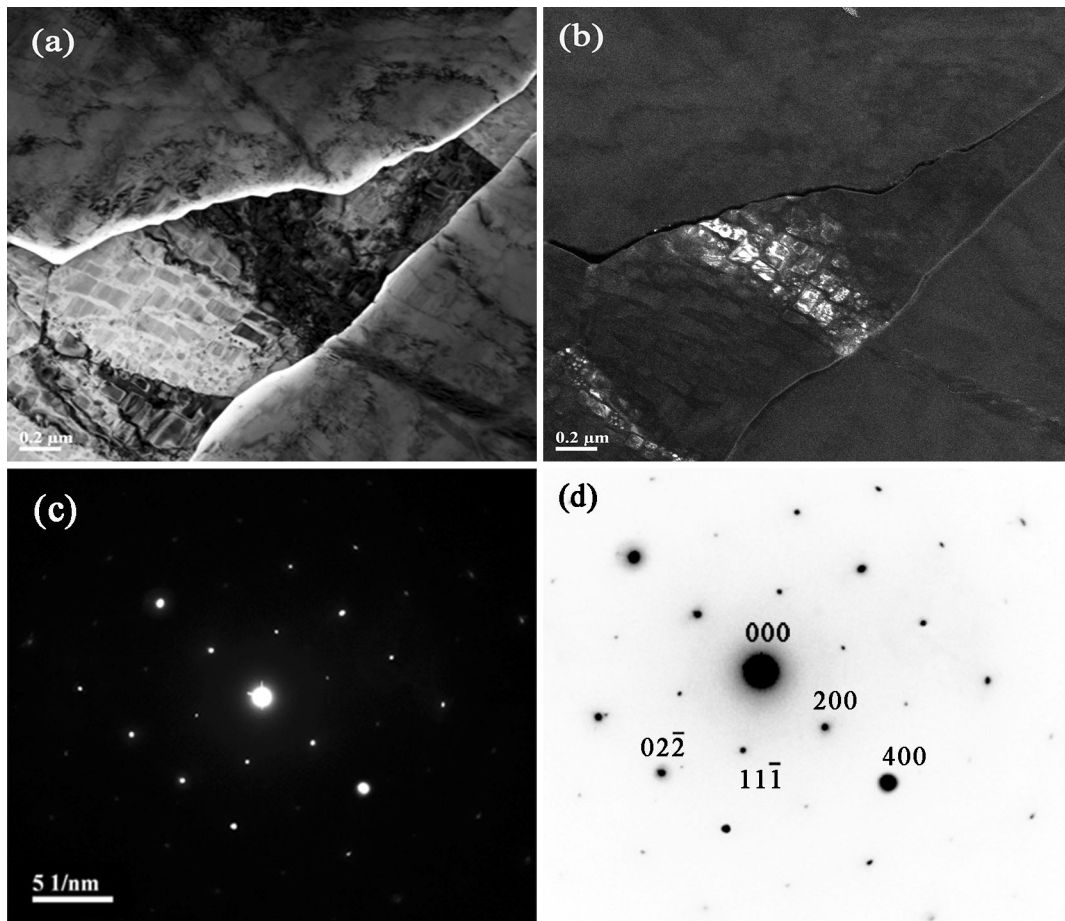


Fig. 10—TEM observation of delta-ferrite in dual-phase manganese steel: (a) bright-field image; (b) dark-field image of (200) ordered spot; (c) diffraction pattern, $[011]_{\text{bcc}}$ zone axis; and (d) indexed pattern in (c) (letter b in subscript representing bcc-ferrite).

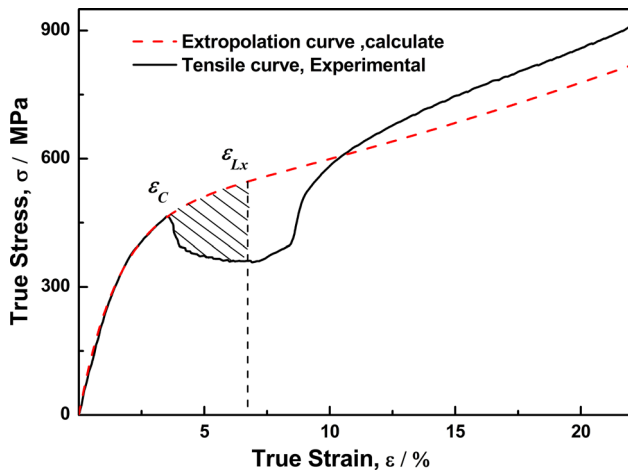


Fig. 11—Illustration of SIM transformation energy measurements.

which is taken as temperature and composition dependency, is fitted, as shown in Figure 13. The resultant interfacial energy as a function of Kelvin's temperature (K) can be expressed by

$$\sigma^{\gamma/\epsilon} = 29.32 - 0.037T \quad [12]$$

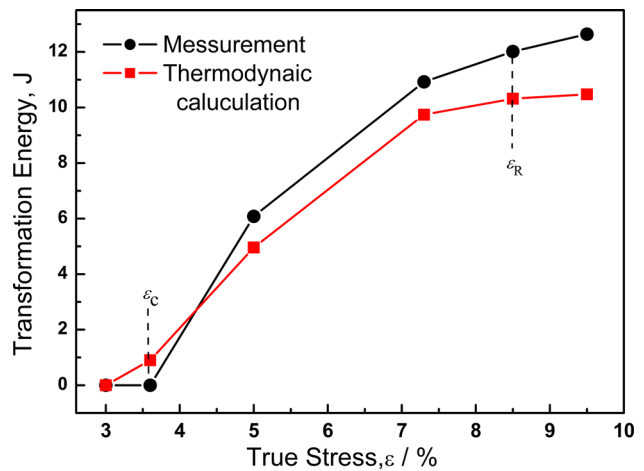


Fig. 12—Comparison of the measured martensitic transformation energy with the thermodynamic calculations at different strain levels.

In this study, the EDS area analysis shows that the composition ranges of elements with Mn, Si, and Al in austenite are 21.8 to 24.6, 1.2 to 2.3, and 2.0 to 2.8 wt pct, respectively, and the average of 20 measurements; Fe-22.8Mn-1.58Si-2.65Al-0.082C (wt pct) is finally taken as the effective composition and used to evaluate

Table I. Deformation Characteristics of the Steel Deformed at Different Temperatures

Deformation Mechanism	Tensile Temperature, K (°C)				
	RT	348 (75)	423 (150)	573 (300)	673 (400)
SIM	●	○	×	×	×
Twinning	●	●	●	○	×

●, Observed, large amount; ○, Observed, small amount; ×, Not observed.

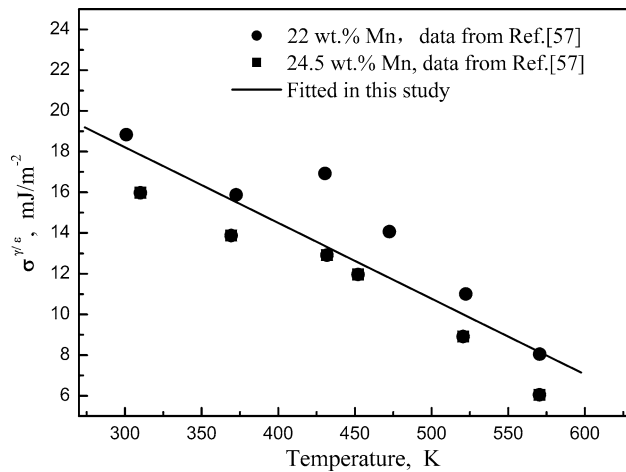


Fig. 13—Change of the interfacial energy with temperature and composition in the Fe-Mn system.

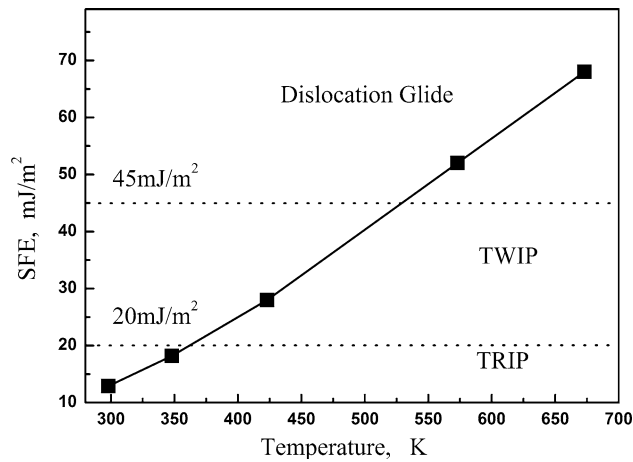


Fig. 14—SFE of austenitic phase in the annealed dual-phase TRIP/TWIP steel as a function of deformed temperatures, in which the dotted line shows the upper limits of the SFE for different deformation modes.

the SFEs of the austenite phase. The resultant SFEs are illustrated in Figure 14.

2. Active plasticity mode at various temperatures

Remy and Pineau^[58] and Sato *et al.*^[59] suggested an SFE value of 20 mJ/m² as the upper limit for the presence of the TRIP mechanism in high-Mn steels, and the plasticity mode may change to deformation twinning when the SFE exceeds this value. Allain *et al.*^[26] believed that the TWIP effect occurred when the SFE was

between 12 and 35 mJ/m². However, plasticity and strain hardening are controlled solely by the glide of dislocations when SFE exceeds 45 mJ/m².^[30] If the SFE values of 20 and 45 mJ/m² are considered as the upper limits for the presentation of the TRIP and TWIP effects, respectively, the resultant SFE values illustrated in Figure 13 clearly show that the annealed dual-phase high-manganese steel in the present study can have a TRIP effect at RT and 348 K (75 °C) deformation and that the TWIP mechanism dominates the 423 K (150 °C) deformation process, while the dislocation glide controls the plasticity at 573 K (300 °C) deformation, consistent with the experimental results summarized in Table I.

IV. CONCLUSIONS

The microstructure evolution and deformation behavior at various temperatures in a high-temperature-annealed dual-phase high-manganese (28 pct δ ferrite-γ austenite) TRIP/TWIP steel were systematically studied in the present work. The main conclusions are as follows.

1. The tensile curves at RT and 348 K (75 °C) exhibit a special Lüders-like yielding phenomenon with a remarkable plastic instability, a large strain plateau, and a plastic re-stability with significantly enhanced work hardening for 1323 K (1050 °C) annealed specimens. However, the tensile curves at 423 K and 573 K (150 °C and 300 °C) deformation show continuous yielding; *i.e.*, no obvious yield drop occurs. The UTS and UE decrease with increasing deformation temperature, except for the specimen at 423 K (150 °C) deformation where ductility is obviously enhanced.
2. A strong TRIP effect takes place during Lüders-like deformation. Semiquantitative analysis of the TRIP effect on the Lüders-like yield phenomenon proves that a softening effect of the strain energy consumption of strain-induced transformation is mainly responsible for this Lüders-like phenomenon.
3. The strain concentration of hard delta-ferrite phase in the dual-phase steel is crucial to the Lüders-like behavior. A delta-ferrite-aided TRIP effect model is proposed to explain this type of Lüders-like phenomenon.
4. The tensile curve in the middle deformation stage exhibits an upward curved behavior, which is closely attributed to the deformation twinning of the part of austenite retained after Lüders-like deformation.

5. The combination of the TRIP effect during Lüders-like deformation and subsequent TWIP effect in the middle stage of deformation greatly enhances the ductility in this annealed high-manganese dual-phase TRIP/TWIP steel.
6. The present annealed dual-phase high-manganese steel can show a TRIP effect at the RT and 348 K (75 °C) deformation; the TWIP mechanism dominates the 423 K (150 °C) deformation process, while the dislocation glide controls the plasticity at 573 K (300 °C) deformation.

ACKNOWLEDGMENTS

The financial support from the Jiangxi Provincial Science and Technology Department (Grant No. 20151BDH80082) and Major Science and Technology Project of Water Pollution Control from the Ministry of Environmental Protection of China (Grant No. 2014ZX07214-002) is gratefully appreciated. One of the authors (LF) acknowledges the financial support from the China Postdoctoral Science Foundation (Grant No. 2015M581608).

REFERENCES

1. O. Grässel, L. Krüger, G. Frommeyer, and L.W. Meyer: *Int. J. Plast.*, 2000, vol. 16, pp. 1391–1409.
2. A. Dumay, J.P. Chateau, S. Allain, S. Migot, and O. Bouaziz: *Mater. Sci. Eng. A*, 2008, vol. 483, pp. 184–87.
3. D. Li, Y. Feng, S. Song, Q. Liu, Q. Bai, F. Ren, and F. Shangguan: *J. Alloys Compd.*, 2015, vol. 618, pp. 768–75.
4. S. Martin, S. Wolf, U. Martin, L. Krüger, and D. Rafaja: *Metall. Mater. Trans. A*, 2016, vol. 47A, pp. 49–58.
5. Y.F. Shen, N. Jia, R.D.K. Misra, and L. Zuo: *Acta Mater.*, 2016, vol. 103, pp. 229–42.
6. S.S. Sohn, H. Song, J.G. Kim, J.H. Kwak, H.S. Kim, and S. Lee: *Metall. Mater. Trans. A*, 2016, vol. 47A, pp. 706–17.
7. H. Ding, H. Ding, D. Song, Z.Y. Tang, and P. Yang: *Mater. Sci. Eng. A*, 2011, vol. 528, pp. 868–73.
8. B.X. Huang, X.D. Wang, Y.H. Rong, L. Wang, and L. Jin: *Mater. Sci. Eng. A*, 2006, vol. 438, pp. 306–11.
9. L.M. Fu, Z.M. Li, H.R. Wang, W. Wang, and A.D. Shan: *Scripta Mater.*, 2012, vol. 67, pp. 297–300.
10. A.H. Cottrell and B.A. Bilby: *Proc. Phys. Soc. A*, 1949, vol. 62 (1), pp. 49–62.
11. S.-J. Kim, C. Gil Lee, T.-H. Lee, and C.-S. Oh: *Scripta Mater.*, 2003, vol. 48, pp. 539–44.
12. N. Tsuchida, Y. Tomota, K. Nagai, and K. Fukaura: *Scripta Mater.*, 2006, vol. 54, pp. 57–60.
13. G.G. Doncel, P. Adeva, M.C. Cristina, and J. Ibañez: *Acta Metall. Mater.*, 1995, vol. 43, pp. 4281–87.
14. G. Tan, Y.N. Liu, P. Sittner, and M. Saunders: *Scripta Mater.*, 2004, vol. 50, pp. 193–98.
15. P. Sittner, Y.N. Liu, and V. Novák: *J. Mech. Phys. Solids*, 2005, vol. 53, pp. 1719–46.
16. Y.N. Liu, Y. Liu, and J.V. Humbeeck: *Scripta Mater.*, 1998, vol. 39, pp. 1047–55.
17. M.R. Barnett, M.D. Nave, and A. Ghaderi: *Acta Mater.*, 2012, vol. 60, pp. 1433–43.
18. E. Emadoddin, A. Akbarzadeh, and G.H. Daneshi: *Mater. Sci. Eng. A*, 2007, vol. 447, pp. 174–79.
19. E. Emadoddin, A. Akbarzadeh, and G.H. Daneshi: *Mater. Charact.*, 2006, vol. 57, pp. 408–13.
20. D.W. Suh, S.J. Park, T.H. Lee, C.S. Oh, and S.J. Kim: *Metall. Mater. Trans. A*, 2010, vol. 41A, pp. 397–408.
21. T.S. Byun, N. Hashimoto, and K. Farrell: *Acta Mater.*, 2004, vol. 52, pp. 3889–99.
22. W.F. Zhang, Y.M. Chen, and J.H. Zhu: *Metall. Mater. Trans. A*, 2002, vol. 33A, pp. 3117–20.
23. W.S. Park, S.W. Yoo, M.H. Kim, and J.M. Lee: *Mater. Des.*, 2010, vol. 31, pp. 3630–40.
24. A.S. Akbari, J. Imlau, U. Prael, and W. Bleck: *Metall. Mater. Trans. A*, 2009, vol. 40A, pp. 3076–90.
25. Y.N. Dastur and W.C. Leslie: *Metall. Trans. A*, 1981, vol. 12A, pp. 749–59.
26. S. Allain, J.P. Chateau, O. Bouaziz, S. Migot, and N. Guelton: *Mater. Sci. Eng. A*, 2004, vol. 387, pp. 158–62.
27. B.X. Huang, X.D. Wang, L. Wang, and Y.H. Rong: *Metall. Mater. Trans. A*, 2008, vol. 39A, pp. 717–24.
28. H. Idrissi, L. Ryelandt, M. Veron, D. Schryvers, and P.J. Jacques: *Scr. Mater.*, 2009, vol. 60, pp. 941–44.
29. X. Tian and Y.S. Zhang: *Mater. Sci. Eng. A*, 2009, vol. 516, pp. 73–77.
30. S. Curtze and V.T. Kuokkala: *Acta Mater.*, 2010, vol. 58, pp. 5129–41.
31. M.N. Shiekhelsouk, V. Favier, K. Inal, S. Allain, O. Bouaziz, and M. Cherkauui: *Mater. Sci. Forum*, 2006, vols. 524–525, pp. 833–38.
32. V. Torabinejad, A.Z. Hanzaki, S. Moemeni, and A. Imandoust: *Mater. Des.*, 2011, vol. 32, pp. 5015–21.
33. A.E. Vidoz and L.M. Brown: *Philos. Mag.*, 1962, vol. 7, pp. 1167–75.
34. B. Bhattacharya, A.S. Sharma, S.S. Hazra, and R.K. Ray: *Metall. Mater. Trans. A*, 2009, vol. 40A, pp. 1190–1202.
35. G.B. Olson and M. Azrin: *Metall. Trans. A*, 1978, vol. 9A, pp. 713–21.
36. T. Gladman, I.D. McIvor, and F.B. Pickering: *J. Iron Steel Inst.*, 1972, vol. 210, pp. 916–30.
37. O. Bouaziz, S. Allain, and C. Scott: *Scripta Mater.*, 2008, vol. 58, pp. 484–87.
38. O. Bouaziz, H. Zurob, B. Chehab, J.D. Embury, S. Allain, and M. Huang: *Mater. Sci. Technol.*, 2011, vol. 27, pp. 707–09.
39. T.Y. Hsu: *Mater. Sci. Eng. A*, 2006, vol. 438, pp. 64–68.
40. A. Perlade, O. Bouaziz, and Q. Furnemont: *Mater. Sci. Eng. A*, 2003, vol. 356, pp. 145–52.
41. J. Wang and S. Zwaag: *Metall. Mater. Trans. A*, 2001, vol. 32A, pp. 1527–39.
42. J.H. Ryu, D.I. Kim, H.S. Kim, H. Bhadeshia, and D.W. Suh: *Scripta Mater.*, 2010, vol. 63, pp. 297–99.
43. T. Inoue and Z.G. Wang: *Mater. Sci. Technol.*, 1985, vol. 1, pp. 845–50.
44. T. Inoue: *Mater. Sci. Forum*, 2009, vol. 614, pp. 11–20.
45. D.P. Koistinen and R.E. Marburger: *Acta Metall.*, 1959, vol. 7, pp. 59–60.
46. G.B. Olson and M. Cohen: *Metall. Trans.*, 1975, vol. 6, pp. 791–95.
47. H. Fujita and S. Ueda: *Acta Metall.*, 1972, vol. 20, pp. 759–67.
48. J.W. Brooks, M.H. Loretto, and R.E. Smallman: *Acta Metall.*, 1979, vol. 27, pp. 1829–38.
49. J.W. Brooks, M.H. Loretto, and R.E. Smallman: *Acta Metall.*, 1979, vol. 27, pp. 1839–47.
50. S. Kajiwaru: *Mater. Sci. Eng. A*, 1999, vol. 273, pp. 67–88.
51. P.H. Adler, G.B. Olson, and W.S. Owen: *Metall. Mater. Trans. A*, 1986, vol. 17A, pp. 1725–37.
52. I. Karaman, H. Sehitoglu, K. Gall, Y.I. Chumlyakov, and H.J. Maier: *Acta Mater.*, 2000, vol. 48, pp. 1345–59.
53. O. Bouaziz and N. Guelton: *Mater. Sci. Eng. A*, 2001, vol. 319, pp. 246–49.
54. S. Chatterjee, H.S. Wang, J.R. Yang, and H.K.D.H. Bhadeshia: *Mater. Sci. Technol.*, 2006, vol. 22, pp. 641–44.
55. J.P. Hirth: *Metall. Trans.*, 1970, vol. 1, pp. 2367–74.
56. Y.K. Lee and C. Choi: *Metall. Mater. Trans. A*, 2000, vol. 31A, pp. 355–60.
57. P.Y. Volosevich, V.P. Gridnev, and Y.N. Petrov: *Fiz. Met. Metalloved.*, 1976, vol. 42, pp. 372–76.
58. L. Remy and A. Pineau: *Mater. Sci. Eng.*, 1977, vol. 28, pp. 99–107.
59. K. Sato, M. Ichinose, Y. Hirotsu, and Y. Inoue: *ISIJ Int.*, 1989, vol. 29, pp. 868–77.